Interannual Variation and Trend of Carbon Budget Observed Over a 28-year Period at Takayama in a Cool-Temperate Deciduous Forest in Central Japan

Shohei Murayama*[1], Hiroaki Kondo[1, 2], Shigeyuki Ishidoya[1], Takahisa Maeda[1], Nobuko Saigusa[3], Susumu Yamamoto[1], Kazuki Kamezaki[1], and Hiroyuki Muraoka[4, 5, 6, 3]

[1] National Institute of Advanced Industrial Science and Technology (AIST), Tsukuba, Japan
[2] Japan Weather Association, Tokyo, Japan
[3] National Institute for Environmental Studies, Tsukuba, Japan
[4] River Basin Research Center, Gifu University, Gifu, Japan
[5] Center for Carbon Neutrality, Environment and Energy, Gifu University, Gifu, Japan
[6] Regional Adaptation Research Center, Gifu University, Gifu, Japan

*Corresponding author: Shohei Murayama (s.murayama@aist.go.jp)

Key Points

- Interannual variations and significant trends of carbon budget components at a forest site were detected from a long-term observation.
- Environmental factors governing the interannual variations and the trend of the annual carbon budget components were investigated.
- Some of the decadal scale phenomena obtained from this study could not be found without the long-term observation.

Abstract

Long-term carbon dioxide (CO_2) flux measurements between the atmosphere and the ecosystem have been made since 1993 at a cool-temperate deciduous forest site (Takayama) in Japan influenced by Asian Monsoon, constituting the longest dataset among all the AsiaFlux sites. Interannual variations (IAVs) and trends of the annual carbon budget components and their environmental factors were examined. Annual net ecosystem production (NEP) (mean ± 1σ) during the period of eddy covariance measurement in 1999-2021 was 265 ± 86 gC m^{-2} yr^{-1}, and its IAV was dependent more on gross primary production (GPP) than on ecosystem respiration. IAVs in annual NEP and GPP were correlated with the IAVs of the monthly mean NEP, GPP and leaf area index (LAI) from June to September, as well as with that of the length of the net carbon uptake period. Significant increasing and decreasing trends in the annual NEP and GPP were detected during 2004-2013 and 2013-2021, respectively; the increasing trends were mainly caused by the vegetation recovery from typhoon disturbances while the decreasing trends were partly influenced by recent extreme weather events. Significant positive correlations of the IAVs between the start and the end of the net carbon uptake period, and between the leaf expansion and leaf fall were found. These may be attributed to biological functions and interseasonal relationship of meteorological parameters associated with ENSO events that can also influence IAVs in annual NEP and GPP.

Plain Language Summary

Forest ecosystems play an important role in the global carbon cycle. However, time variations in the ecosystem carbon budget and its responses to climate change are not well understood. Although long-term observational data are useful for a better understanding, >20-year observations are limited, especially in the Asian monsoon region. In this study, long-term measurements of carbon budget made at a cool-temperate deciduous forest in Japan were analyzed for interannual variation (IAV), long-term trends, and offered plausible causes for these changes. The IAV in annual net carbon uptake (NEP) was associated with the variation in summertime NEP, as well as with the variation in the length of the net carbon uptake period (NGP). The IAV in summertime NEP was associated with the variations in solar radiation (SR) and leaf density during the season, while the IAV in NGP length depended on the variations in spring temperature and early-fall SR. Decadal increasing and decreasing trends of annual NEP were also detected. The former was mainly caused by recovery from typhoons, while the latter was likely related to recent extreme weather events. Longer-term ecosystem observations are certainly needed for more accurate predictions of forest ecosystems response to climate change.

1. Introduction

Terrestrial biosphere is one of the most important reservoirs in the global carbon cycle. Various changes in terrestrial biosphere caused by climate change and atmospheric carbon dioxide (CO_2) increase have been discussed in many recent studies (e.g., Friedlingstein et al. 2022; Piao et al. 2019a; Reichstein et al. 2013). Extension of the growing season due to warmer climate and enhanced fertilization effects have caused increase in CO_2 uptake by the terrestrial ecosystems, while enhancement of respiration and decomposition of organic matters due to warmer climate have resulted in an increase in CO_2 release (IPCC, 2021). On a shorter and local scale, disturbance of ecosystem functions due to increase in frequency of extreme weather accompanied by climate change can affect the carbon budget (e.g., Reichstein et al. 2013). Given that East Asia is strongly influenced by the Asian Monsoon, any change in the temperature and precipitation amount, along with the length of the rainy season, associated with the monsoon can have a major impact on the terrestrial carbon budget. The present research addresses some of these issues.

Various networks of CO_2 flux measurements between the atmosphere and the terrestrial ecosystems have been developed since 1990's (e.g., Wofsy et al., 1993; Baldocchi et al., 2001). Understanding of the environmental factors causing carbon flux changes and the development of terrestrial carbon cycle models all benefited from the measurements obtained from these networks (e.g., Musavi et al., 2017). In particular, long-term data are employed to contribute to the reduction of uncertainty in statistical analyses of the interannual variations (IAV) and the secular trend (Baldocchi et al., 2018). Thus, decadal-scale study should be conducted by combining micro-meteorological observation and ecological research (Ito et al. 2015; Muraoka et al. 2015). However, the long-term measurements of >20 years are still limited, especially in the Asian monsoon region.

Long-term measurements of CO_2 flux between the atmosphere and the forest ecosystem, and the atmospheric CO_2 mixing ratio in and above the canopy have been made since September 1993 at Takayama site (TKY) in a cool-temperate deciduous forest in central Japan (Yamamoto et al., 1999; Saigusa et al., 2002; Murayama et al., 2003). TKY has the longest flux data among the AsiaFlux sites (https://www.asiaflux.net/). Also, the continuous measurement of the atmospheric O_2/N_2 ratio, along with the measurement of the atmospheric CO_2 isotopic ratios using a flask sampling method have been conducted at the site (Ishidoya et al., 2015; Murayama et al., 2010). Various analyses of the data have been conducted to obtain a better understanding of the IAV in annual carbon budget related to Asian Monsoon and ENSO events (Saigusa et al., 2005, 2008; Yamamoto et al., 1999).

In this study, the longer-term data between 1994 and 2021 (mainly between 1999 and 2021) are reanalyzed to investigate the decadal changes in the IAV and the trend of annual carbon budget associated with observed climatic and ecological mechanisms. We will examine the relationship of the IAV in the annual carbon budget with those in the summertime carbon uptake (Subsection 4.1) and the net carbon uptake period (Subsection 4.2), on the assumption that the annual carbon budget is largely affected by these parameters. We will further examine the trend of the annual carbon budget and its causes, such as disturbances of the forest and meteorological trends (Subsection 4.3). We will also examine the impact of recent extreme weather on the carbon budget. Based on these results, climatic and ecological mechanisms governing the IAV (Subsection 5.1) and the trend (Subsection 5.2) of the annual carbon budget will be discussed by comparing with the previous studies of other forest sites, as well as TKY. We will also discuss influences of interseasonal factors and El Niño-Southern Oscillation (ENSO) on the IAV and a decadal trend of the annual carbon budget (Subsection 5.3).

2. Method

2.1. Site descriptions

Detailed descriptions of our observation site have already been given in our previous papers (Yamamoto et al., 1999; Saigusa et al., 2005; Murayama et al., 2010). Our observation site, TKY is located in a mountainous area in the central part of the main island of Japan (36°09'N, 137°25'E, 1420 m a.s.l.) and is situated about 15 km east of a local city, Takayama. TKY is part of observation networks such as AsiaFlux (http://asiaflux.net/index.php?page_id=112) and Japan Long-Term Ecological Research network (JaLTER: http://www.jalter.org/en/). Vegetation at the site is a 60 to 70-year-old secondary deciduous broadleaf forest primarily dominated by birch (*Betula ermanii* Cham and *B. platyphylla* Sukatchev var. *japonica* Hara) and oak (*Quercus crisplula* Blume). The canopy height is about 15-20 m. The forest understory is dominated by an evergreen dwarf bamboo (*Sasa senanensis* Rehd.) (Muraoka & Koizumi, 2005; Ohtsuka et al., 2007). Leaf expansion and leaf fall of broadleaf trees occur in May and in October or November, respectively, and the ground surface is usually covered with snow from December to April. Annual mean temperature and precipitation amount averaged over 1994-2021 are about 6.7°C and 2200 mm, respectively. The rainy season is strongly influenced by the Asian Monsoon and usually occurs in early summer (June – July). Possible effects of nearby anthropogenic sources on the data observed at our site were estimated by Kondo et al. (2001) using a numerical model and were found to be relatively minimal.

2.2. Observation

Since detailed descriptions of our CO_2 flux and atmospheric CO_2 mixing ratio measurements have been given in our previous papers (Yamamoto et al., 1999; Saigusa et al., 2002, 2005; Murayama et al., 2003, 2010), only a brief and supplemental explanation will be presented here.

The continuous measurements of the CO_2 flux and the atmospheric CO_2 mixing ratio have been made using a 27-m height tower located on the top of a small hill. Meteorological parameters such as downward and upward shortwave and longwave radiations, air temperature, relative humidity, wind speed, and its direction were also measured on the tower. Photosynthetic active radiation (PAR) was measured above and below the tree canopy (but above the canopy of dwarf bamboo) using quantum sensors (IKS-27, KOITO and/or SQ-110, APOGEE). The daily LAI of the tree canopy not including the dwarf bamboo was estimated as follows:

$$LAI = -\frac{1}{K}\left(ln\frac{PAR_b}{PAR_a} - ln\frac{PAR_{b0}}{PAR_{a0}}\right), \quad (1)$$

where PAR_b and PAR_a denote daily summed values of the downward PAR measured below and above the canopy, PAR_{b0} and PAR_{a0} denote those averaged for the period of DOY (day of the year) 100-120 before starting leaf expansion, and K denotes the extinction coefficient. Here, we set K to a constant value (0.46) based on the estimation for TKY (Muraoka et al., 2010; see also Nasahara et al. 2008, Saitoh et al. 2012). The obtained LAI values were often scattered day by day. Therefore, we used their 10-day running mean values for the further analyses in relation to the CO_2 flux. Since some problems with the PAR measurement below the tree canopy occurred in 2019, the LAI data for the year were not used for analyses in this paper. Precipitation was measured at a site located about 400 m from the tower by the River Basin Research Center (RBRC), Gifu University.

The CO_2 flux measurement started by an aerodynamic (AD) method and an eddy covariance (EC) method in September 1993 and July 1998, respectively. The hourly CO_2 flux by AD method was estimated from the vertical gradient of the hourly mean CO_2 mixing ratio between two heights above the canopy (27 and 18 m). The CO_2 mixing ratio was measured by a non-dispersive infrared (NDIR) analyzer (Model 880, Rosemount or LI-6252, Li-Cor) with precision of better than 0.1 ppm. The CO_2 flux data by the AD method were intensively compared with those by the EC method between July 1998 and December 2000 (Saigusa et al., 2005). The relationship between both methods was obtained from the comparison of the daily values. The daily CO_2 flux data by the AD method were adjusted to those by the EC method using the relationship during the period before the start of the EC measurement.

The CO_2 flux measurement by the EC method at 25 m on the tower was made using a three-dimensional ultrasonic anemometer (DAT-600, Kaijo) and a closed-path NDIR (LI-6262, Li-Cor). Detailed descriptions of the eddy covariance method were given in Saigusa et al. (2002). The net ecosystem CO_2 exchange (NEE) was calculated every half-hour taking account of the CO_2 storage in the canopy. Small data gaps of up to 2-3 h were filled by linear interpolation. Large gaps were filled by empirical equations expressing the relationship among NEE, air temperature and incident PAR above the tree canopy shown in Saigusa et al. (2002, 2005).

Drainage flow along the slope often occurred in calm nights at TKY, and the NEE measured by the EC method was likely underestimated during the nighttime under the stable atmospheric conditions. To avoid the flux underestimation, the NEE values at the stable nights had been replaced by an empirical exponential formula throughout the year obtained from the relationship between the air temperature at 25-m height and the ecosystem respiration (Rec) at the site measured by the eddy covariance method under nearly neutral atmospheric stability conditions in Saigusa et al. (2002, 2005). In this study, the relationship between the air temperature (T (°C)) at 25-m height and Rec (μmol m^{-2} s^{-1}) was reanalyzed using the long-term data. Because its seasonal difference of the relationship was found from the reanalysis, the following empirical formulas were used to estimate Rec (nighttime NEE) under the stable atmospheric conditions (friction velocity (u*) < 0.5 m s^{-1}) for each period of the year:

$Rec = 2.37 \times 3.42^{\frac{T-10}{10}}\ (T < 15),\ Rec = 4.39\ (T \geq 15),$ for April and May, (2)

$Rec = 0.0821T + 2.74,$ for June and July, (3)

$Rec = 0.110T + 1.59,$ for August and September, (4)

$Rec = 2.11 \times 1.87^{\frac{T-10}{10}}\ (T < 16), Rec = 3.06\ (T \geq 16),$ for October and November, (5)

$Rec = 0.0232T + 0.667,$ for December to March. (6)

In this study, we assumed that the temperature dependence of daytime Rec was the same as that of nighttime Rec, though problems with the assumption have been pointed out in some studies (e.g., Reichstein et al., 2005; Wehr et al., 2016).

In the following analyses, daily (24 h) carbon budget components were calculated as follows. The daily net ecosystem production (NEP) was assumed to be the negative quantity of the daily NEE:

$NEP = -NEE.$ (7)

The daily gross primary production (GPP) was derived from NEP and Rec:

$GPP = NEP + Rec.$ (8)

3. Data analyses

In order to examine the IAV in the seasonal cycle of NEP, we obtained the best fit curve to the daily NEP data by employing the curve fitting technique described in Nakazawa et al. (1997). In this iterative procedure, the fundamental and its first to third harmonics (a four-harmonic fit) were used.

The occurrences of the NEP growing start (NGS) and end (NGE) were defined by the intersections of the above-mentioned best fit curve and the zero line from the negative value to the positive one (net CO_2 release to uptake) and from the positive value to the negative one (net CO_2 uptake to release), respectively. The interval between the NGS and the NGE, which is the net carbon uptake period, was also defined as the NEP growing period (NGP).

4. Results

In Fig. 1a, the daily NEP and the best fit curve to these data are shown for 1994-2021. Although day-to-day NEP is largely scattered, the NEP often shows positive values (CO_2 uptake) and negative values (CO_2 release) from late spring to early fall and the remaining period, respectively. Obvious positive peaks in summer and large IAV in the peak height are seen from the fitting curve. On the other hand, relatively weak CO_2 release is seen from late fall to early spring, and the IAV in the CO_2 release during these periods is very smaller than that in the CO_2 uptake peak.

Figure 1b shows temporal variations of monthly mean of the estimated carbon budget components. The monthly mean data are also given in the Supporting Information (Tables S1-S3). Each component has sharp peaks in summer and broad troughs in cold seasons, though small sharp troughs are seen late in fall and/or in early spring in some years. The IAV in the summer peak height of GPP is larger than that of Rec. Therefore, the IAV in the summer peak height of NEP is mainly due to that of GPP.

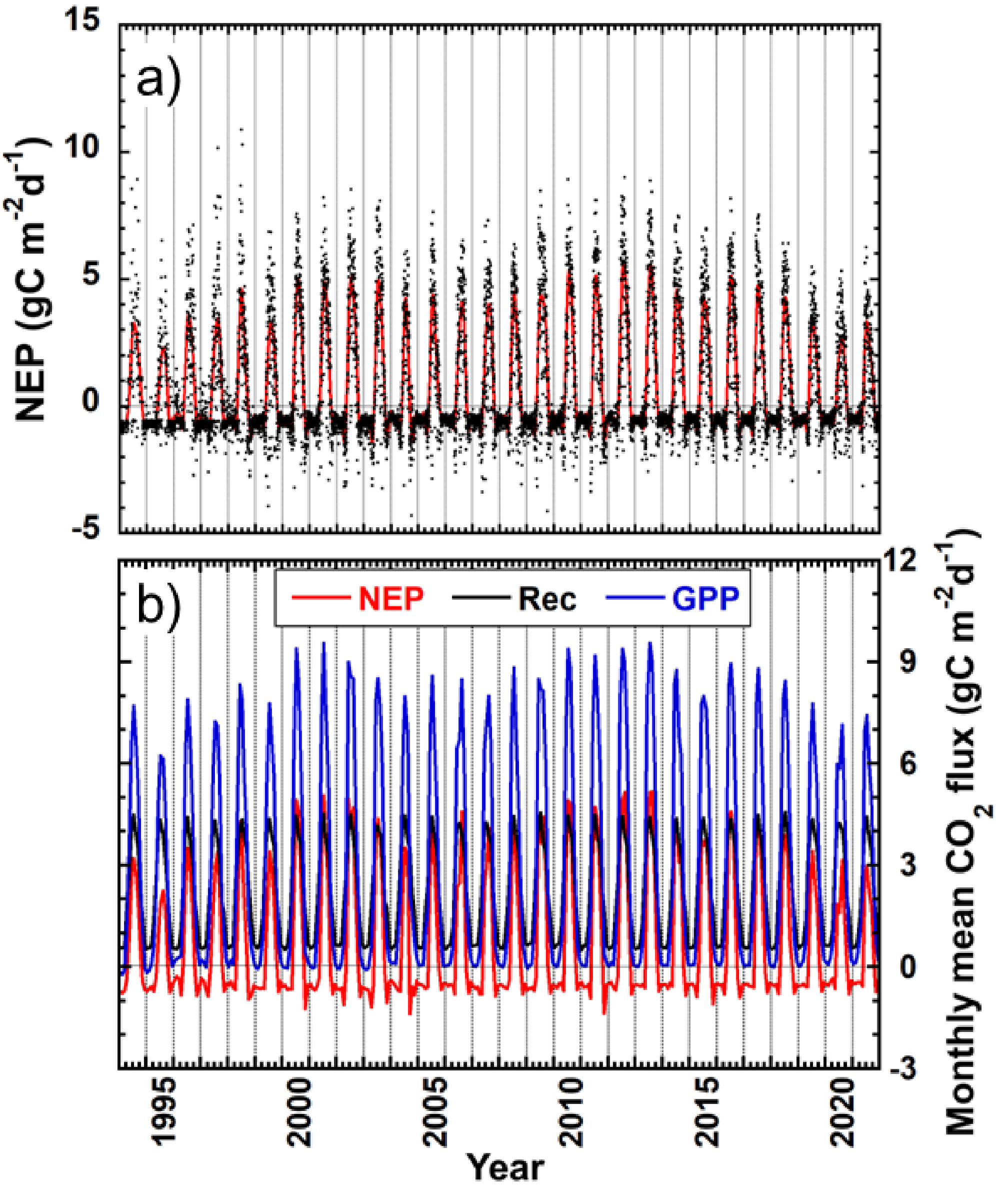

Figure 1. a) Temporal variation in daily NEP (dot) and the best fit curve to the data (red line) for 1994-2021. b) Temporal variations in monthly mean daily NEP (red line), Rec (black line) and GPP (blue line) for the same period.

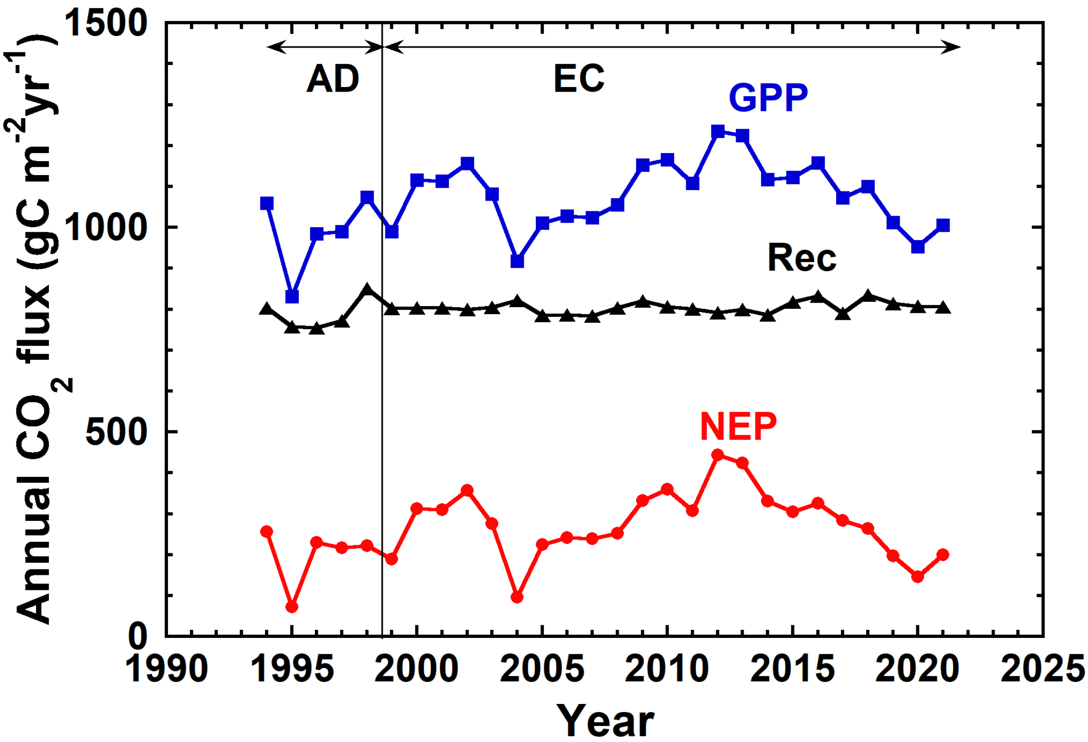

Figure 2. Temporal variations in annual NEP, Rec and GPP. The data were obtained by using an aerodynamic (AD) method and an eddy-covariance (EC) method until July 1998 and after that, respectively.

Figure 2 shows variations of the estimated annual carbon budget components. The data of the annual carbon budget components are also given in the Supporting Information (Table S1-S3). The IAV is much larger for annual NEP and GPP than for annual Rec. The average values and the standard deviations (1σ) of annual NEP, GPP and Rec for 1994-2021 were 265 ± 86, 1066 ± 91, and 801 ± 21 gC m^{-2} yr^{-1}, respectively. For the EC observation period of 1999-2021, they were 279 ± 83, 1083 ± 82, and 804 ± 14 gC m^{-2} yr^{-1}, respectively. The fact that the IAV pattern of the annual NEP is similar to that of the annual GPP suggests that the IAV in the annual NEP depends largely on the IAV in the annual GPP at TKY. The annual NEP and GPP both show increases from the late 1990s to early 2000s, rapid decreases in 2004, gradual increases from 2004 to the early 2010s, and then gradual decreases in the late 2010s. The rapid decreases of the annual NEP and GPP in 2004 were related to disturbances of the forest ecosystem due to typhoon strikes, as suggested by fairly lower LAI values from June to October in 2004 compared to the averaged values (Fig. S1). Ten typhoons landed in the Japanese Islands from June to October in that year (Ito, 2010a), which were more than three times the average annual landfalls in Japan over the 1991-2020 period (https://ds.data.jma.go.jp/gmd/cpd/longfcst/en/tourist_tc.html).

The IAVs of the maximum NEP during the summertime and the length of the NGP can strongly influence the IAV of the annual NEP, as illustrated in Fig. 3. In the following sections, factors governing IAVs and trends of annual carbon budget components will be analyzed based on this concept. To avoid systematic difference between AD and EC measurements, the following statistical analyses of the carbon budgets will mainly employ the EC data obtained during the period of 1999-2021. Some statistical analyses will be limited to 1999-2017 to

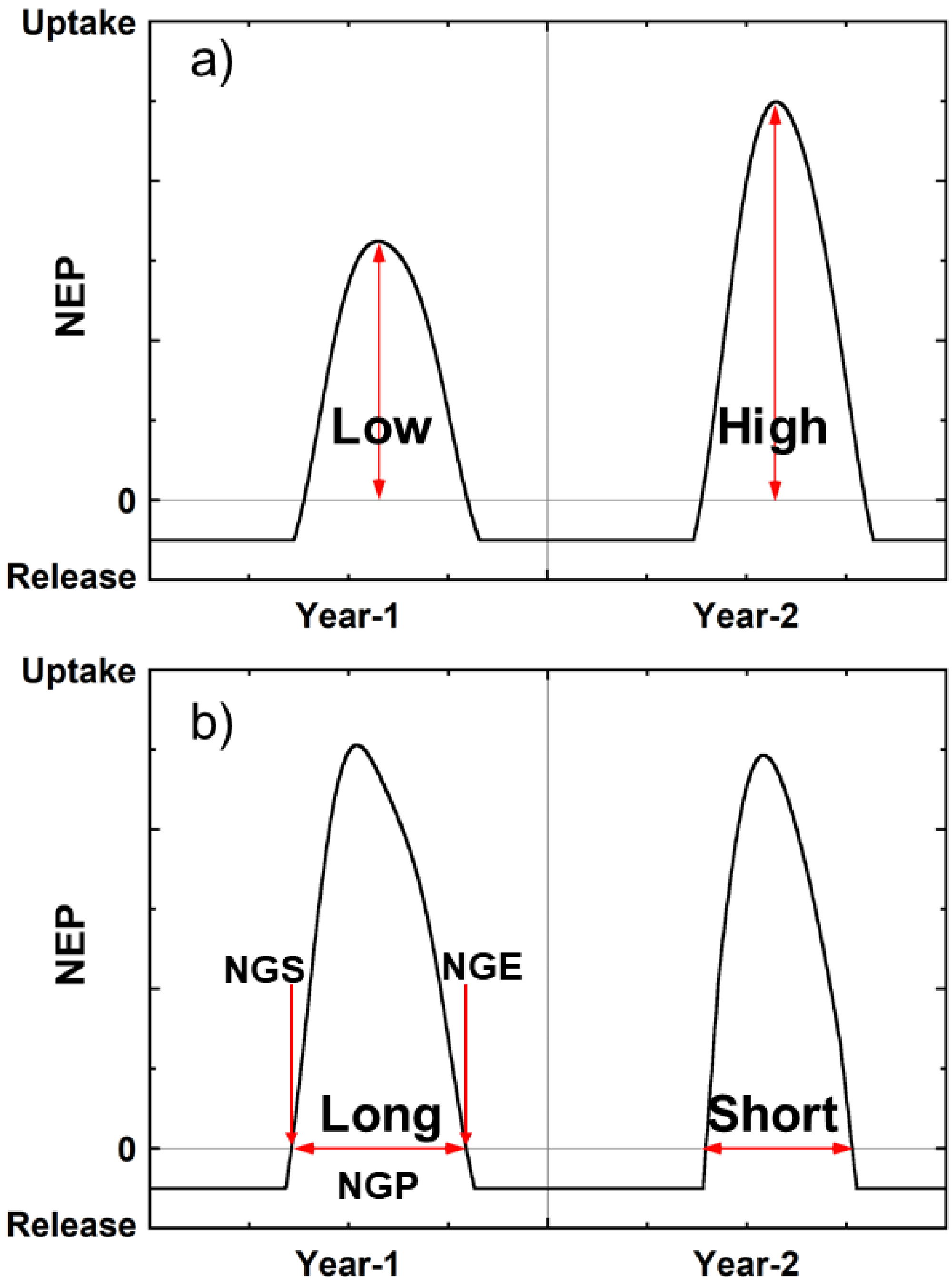

Figure 3. Schematic diagram showing factors governing the IAV in annual NEP; a) the IAV in the magnitude of the NEP during the summertime, and b) that in the length of the period (NGP) showing positive NEP values (between the NGS and the NGE).

exclude possible impacts of increase in the frequency of recent extreme weather events described later.

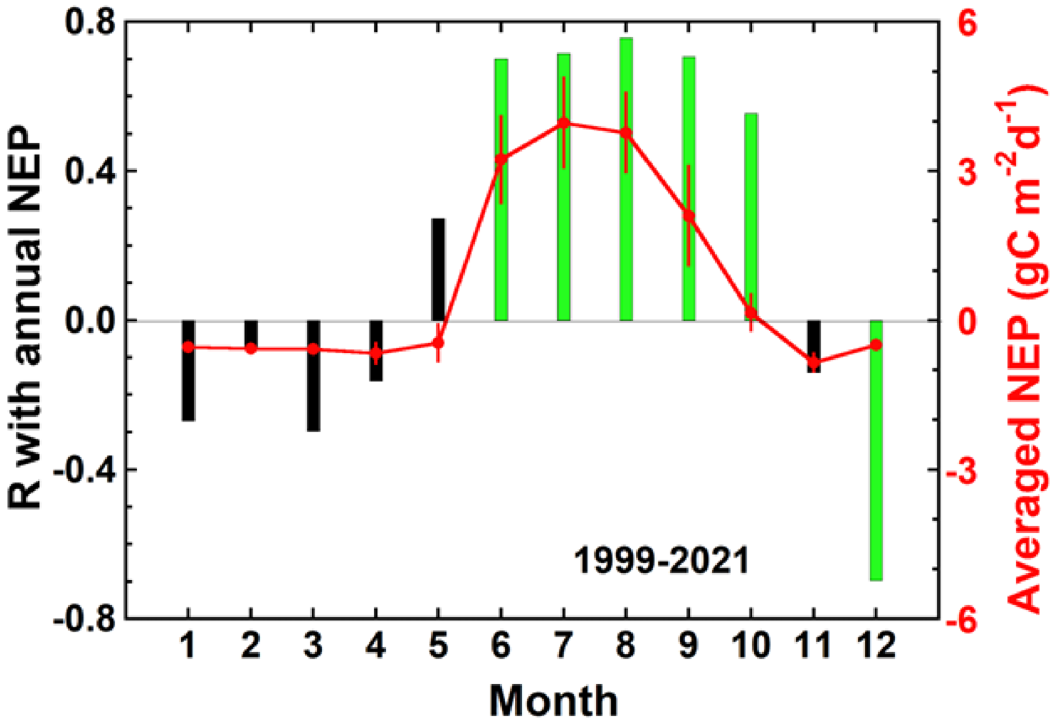

Figure 4. Correlation coefficients (R) of the IAV between annual NEP and monthly mean NEP for each month for 1999-2021 (green and black vertical bars), and the averages of monthly mean NEP for each month over 1999-2021 (red closed circles) along with the standard deviation (1σ) from the average values (red vertical lines). The green bars represent significant correlations at >99% confident levels.

4.1. Influence of summertime IAV in carbon uptake on annual NEP and GPP variability

Since photosynthetic activities are largely enhanced during the summertime, it can be hypothesized that the IAV in strength of carbon uptake in summer contributes to the IAVs of the annual NEP and GPP. To examine this hypothesis, correlations of the IAV between the annual NEP and monthly mean NEP for each month were analyzed for the period 1999-2021. In Fig. 4, the correlation coefficients (R) for each month are shown. The average values of monthly mean NEP, along with the standard deviation (1σ) from the average values, are also shown in this figure. With the exception of December, statistically significant positive correlations of the IAV between the annual NEP and monthly mean NEP for each month from June to October are found ($P < 0.01$). Especially from June to September, the average values of the monthly mean NEP show large net CO_2 uptake (> 2 gC m^{-2} d^{-1}) and IAV ($\sigma > 0.8$ gC m^{-2} d^{-1}). Similar significant correlations ($P < 0.01$) of the IAV were found between annual GPP and monthly mean GPP for each month from June to September, when the average values of the monthly mean GPP (>5 gC m^{-2} d^{-1}) and the IAVs (σ > 0.8 gC m^{-2} d^{-1}) were large. These results suggest that the IAVs in NEP and GPP from June to September make significant contributions to the IAVs observed in annual NEP and GPP.

Table 1. Correlation coefficient of IAVs of monthly mean SR in June, July, August and September with those of monthly mean NEP and GPP for the respective months in1999-2021 and 1999-2017 except for 2004.

	June	July	August	September
NEP 1999-2021	0.22	0.67***	0.46**	0.64***
1999-2017	0.31	0.62***	0.68***	0.58**
GPP 1999-2021	0.22	0.71***	0.51**	0.59***
1999-2017	0.30	0.65***	0.70***	0.50**

Note: ** and *** represent statistical significance of correlations for $0.05 < P \leq 0.01$ and $P < 0.01$, respectively.

Table 1 shows correlation coefficients (R) with the IAVs in monthly mean solar radiation (SR) for each month in 1999-2021 and 1999-2017. In this analysis, the data for 2004 were not included since the forest ecosystem around our site was disturbed by typhoons from June to October. The correlations are also shown in Fig. S2. Significant positive correlations are found for each month from July to September for 1999-2021 and 1999-2017, while significant correlations are not found for June. With respect to August, the R values for 1999-2021 decrease by almost 0.2, compared to those for the period 1999-2017.

Next, we carried out correlational analyses of the IAVs in NEP and GPP with LAI. In addition to the analyses of the IAVs in monthly mean LAI for each month from June to September with the IAVs of the monthly mean NEP and GPP for respective months, we also conducted the same analysis with the IAVs of the annual NEP and GPP of the corresponding year. In this analysis, the data for 2019 were excluded due to the problem with the PAR measurement during the year, as mentioned above. The results are shown in Table 2 and Fig. S3. The correlations of the IAVs in monthly mean LAI with those of monthly mean NEP and GPP from June to September of 1999-2017 and for June, August and September of 1999-2021 are significantly positive for each month. The statistical significance for June-August of 1999-2021 are less compared to those of 1999-2017. The IAVs in the monthly mean LAI for the respective months of June to September also show significantly positive correlations with those in the annual NEP and GPP, and each of the correlations shows larger significance in 1999-2017 than in 1999-2021.

Table 2. Correlation coefficients (R) of IAV in monthly mean LAI for each of June, July, August and September with those in monthly mean NEP and GPP for the respective months and with those in annual NEP and GPP in the same year in 1999-2021 except for 2019 and in 1999-2017.

	June	July	August	September
Monthly NEP				
1999-2021	0.58***	0.31	0.44**	0.78****
1999-2017	0.79****	0.58***	0.64***	0.82****
Monthly GPP				
1999-2021	0.59***	0.30	0.45**	0.77****
1999-2017	0.77****	0.56**	0.63***	0.80****
Annual NEP				
1999-2021	0.36*	0.55***	0.61***	0.61***
1999-2017	0.66***	0.77****	0.83****	0.82****
Annual GPP				
1999-2021	0.46**	0.59***	0.64***	0.58***
1999-2017	0.72****	0.78****	0.84****	0.80****

Note: *, **, *** and **** represent statistical significance of correlations for $0.1 < P \leq 0.05$, $0.05 < P \leq 0.01$, $0.01 < P \leq 0.001$ and $P < 0.001$, respectively.

4.2. Influence of IAV in NGP on those in annual NEP and GPP

The IAV in the NGP can also contribute to the IAVs in the annual NEP and GPP. Earlier occurrence of the NGS and/or later occurrence of the NGE can result in a longer NGP, and it can cause increase in annual NEP. In Table 3, the R values of the IAVs in annual NEP and GPP with those of the NGS and NGE and the length of the NGP of the respective years in 1999-2021 and 1999-2017 are shown. In the analysis, the data of 2004 are not included due to the above mentioned reason. The correlations of IAVs in NGS, NGE and NGP with those in annual NEP and GPP are also shown in Fig. S4. The IAVs in the annual NEP and GPP show significant positive correlation with the IAV in NGP for both 1999-2021 and 1999-2017 though the correlations are much more significant in 1999-2017 than in 1999-2021 periods. Significant negative correlations of IAV in NGS with that in annual GPP for both periods and significant positive correlations of IAV in NGE with those in annual NEP and GPP for 1999-2017 are also shown.

Table 3. Correlation coefficient (R) of IAVs in NGS, NGE and NGP with those of annual NEP and GPP and environmental factors for 1999-2021 and 1999-2017.

	Parameter	R	
		1999-2021	1999-2017
NGS	Annual NEP	-0.34	-0.38
	Annual GPP	-0.45**	-0.46*
	T_spring	-0.75****	-0.81****
	LE_{LAI}	0.83****	0.80****
	LE_{CET}	0.81****	0.80****
NGE	Annual NEP	0.30	0.57**
	Annual GPP	0.20	0.46*
	SR_SEP	0.70****	0.68***
	LAI_SEP	0.38*	0.29
	LF_{LAI}	0.58***	0.51**
	LF_{CET}	0.30	0.24
NGP	Annual NEP	0.57***	0.75****
	Annual GPP	0.58***	0.72****
	T_spring	0.39*	0.40*
	SR_SEP	0.44**	0.56**
	LAI_SEP	0.45**	0.61***

Note: T_spring is mean T from March to May. SR_Sepetmber and LAI_September are monthly mean SR and LAI in September, respectively. The data of 2004 are excluded in this analysis. The data of LE_{LAI}, LF_{LAI} and LAI_September for 2019 are also excluded in this analysis. *, **, *** and **** represent statistical significance of correlations for $0.1 < P \leq 0.05$, $0.05 < P \leq 0.01$, $0.01 < P \leq 0.001$ and $P < 0.001$, respectively.

We then proceeded to examine the possible impacts of the plant phenological events such as leaf expansion (LE) and leaf fall (LF) of canopy trees and environmental factors on NGS, NGE and NGP. In this study, the first day of the year that LAI exceeded 50% of the average value of LAI over DOY 180-240 (i.e., local summer) of the year, when the LAI values were fairly stable and the maximum of the year appeared, was defined as an indicator (LE_{LAI}) of the occurrence of LE. Such simplified indicator allows us to examine the IAV in forest canopy phenology and its impacts on CO_2 flux. Similarly, the first day of the year that LAI fell below 50% of the average value of the LAI over DOY 180-240 of the year was defined as an indicator (LF_{LAI}) of the occurrence of LF. Furthermore, we also calculated the occurrences of LE and LF of canopy trees of each year using a degree-day model of vegetation phenology by Nagai et al. (2021). In the model optimized to reproduce the phonology events at TKY, the LE date (LE_{CET}) was defined as the first day when the cumulative effect temperature (CET) was greater than

255.4˚C. The CET$_{st}$ was calculated with Eq. (9), where T$_i$ is the daily mean air temperature (˚C) at 25-m height, and we set the start date to be January 1st and the threshold temperature for the CET to be 2˚C.

$$CET_{st} = \sum_{i=Jamuary\ 1}^{LE_{CET}} \max(T_i - 2, 0), \quad (9)$$

The LF date (LF$_{CET}$) was also defined as the first day when the CET was less than −375.1˚C. The CET$_{en}$ was calculated with Eq (10), where we set the start date to be August 1st and the threshold temperature for the CET to be 18˚C.

$$CET_{en} = \sum_{i=August\ 1}^{LF_{CET}} \min(T_i - 18, 0), \quad (10)$$

Note that the occurrences of LE$_{CET}$ and LF$_{CET}$ are earlier and later than those of LE$_{LAI}$ and LF$_{LAI}$, respectively since the LE$_{CET}$ and the LF$_{CET}$ are the parameters to estimate the start of leaf expansion and the end of leaf fall, respectively (Nagai et al., 2013). Also, factors other than air temperature such as impacts of disturbances of the forest ecosystem are not considered in the model. The correlations of the IAVs in NGS, NGE and NGP with those in the LE$_{CET}$ and the LF$_{CET}$ were also examined. The IAVs in the occurrences of LE$_{LAI}$, LF$_{LAI}$, LE$_{CET}$ and LF$_{CET}$ thus obtained along with those of NGS and NGE are shown in Fig. 5. As described above, the occurrences of LE$_{LAI}$ and LF$_{CET}$ are later than those of LE$_{CET}$ and LF$_{LAI}$, respectively. It can also be seen in the figure that the occurrences of NGS and NGE are closer to those of LE$_{CET}$ and LF$_{LAI}$ than those of LE$_{LAI}$ and LF$_{CET}$, respectively in most of the years during the 1999-2021 period. In 2004 when the disturbances due to typhoons occurred, NGE occurred very earlier than the other years.

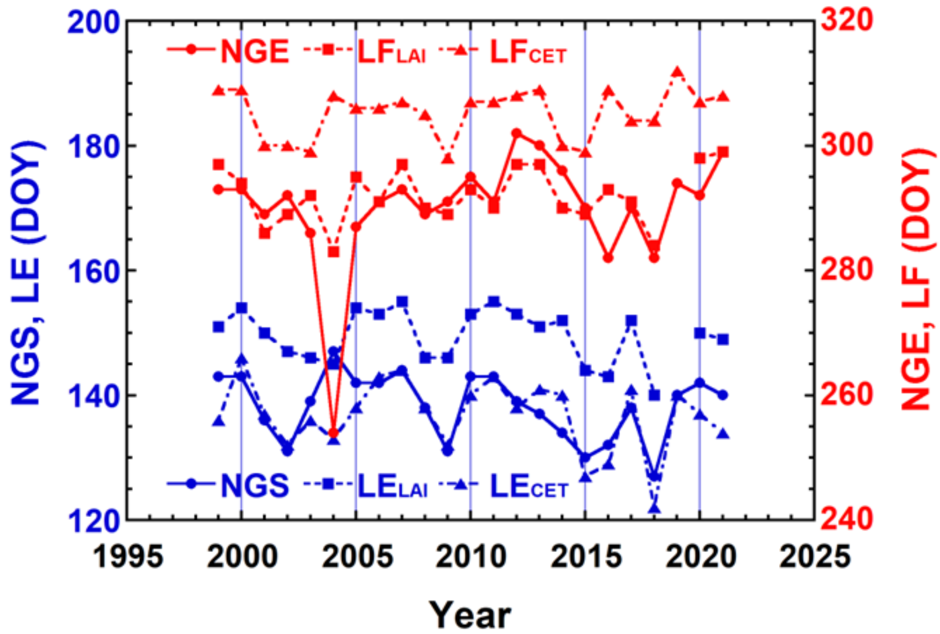

Figure 5. IAVs in occurrences of NGS, NGE, LE$_{LAI}$, LF$_{LAI}$, LE$_{CET}$ and LF$_{CET}$. LE$_{LAI}$ and LF$_{LAI}$ for 2019 are not plotted because of no available LAI data.

Correlations of the IAV in NGS, NGE and NGP with those in environmental factors are also shown in Table 3 and Fig. S5. The IAV in the occurrence of NGS is significantly negatively and positively correlated with those in the mean air temperature from March to May (T_spring) and the occurrences of LE (LE_{LAI} and LE_{CET}), respectively. Significantly positive correlations of the IAV in the occurrence of the NGE are also found with those in the occurrence of LF_{LAI} and the monthly mean SR (SR_SEP) and LAI (LAI_SEP) in September though the correlations with LAI_SEP for 1999-2017 and the occurrence of LF_{CET} are not significant. With respect to the NGP, its IAV shows significantly positive correlations with those in T_spring, SR_SEP and LAI_SEP.

4.3. Trends of annual carbon budget components and their environmental factors

Figure 2 shows a linear increasing trend in the annual Rec during the period of 1994-2021 (0.90 ± 0.47 (1σ) gC m^{-2} yr^{-1} yr^{-1}, R = 0.35, P < 0.1) based on both the EC and AD data. This trend may be partly attributed to a significant increasing trend of annual mean air temperature observed at TKY during the period (+0.045 ± 0.012 (1σ) °C yr^{-1}, R = 0.59, P < 0.01). However, no significant linear trends were found in annual NEP and GPP IAVs over the same period. Also, no significant linear trends were found in IAVs of annual NEP, GPP and Rec for the EC observation period of 1999-2021. On the other hand, significantly increasing trends in annual NEP (31.9 ± 4.5 (1σ) gC m^{-2} yr^{-1} yr^{-1}, R = 0.94, P < 0.001) and GPP (31.8 ± 4.0 (1σ) gC m^{-2} yr^{-1} yr^{-1}, R = 0.94, P < 0.001) in 2004-2013 were found, while significantly decreasing trends were detected in annual NEP (-28.8 ± 4.2 (1σ) gC m^{-2} yr^{-1} yr^{-1}, R = 0.93, P < 0.001) and in GPP (-27.4 ± 5.2 (1σ) gC m^{-2} yr^{-1} yr^{-1}, R = 0.89, P < 0.01) for the period 2013-2021.

Figure 6 shows IAVs in the monthly mean NEP and GPP of each month from June to September, as well as NGS, NGE and NGP. The monthly mean NEP (Fig. 6a) and GPP (Fig. 6b) values of June and from July to September show significantly increasing trends during 2004-2016 and 2004-2013, respectively, while significantly decreasing trends are found from June to September in 2013-2021. Figure 6c shows a significant trend pointing to an ever earlier occurrence of NGS (2004-2018), as well as to an ever later occurrence of NGE (2005-2013). As a result, a significantly increasing trend of NGP is also seen (2005-2013). It is interesting to note that the NGE trend reverses from 2013 to 2018, indicating an earlier occurrence each year.

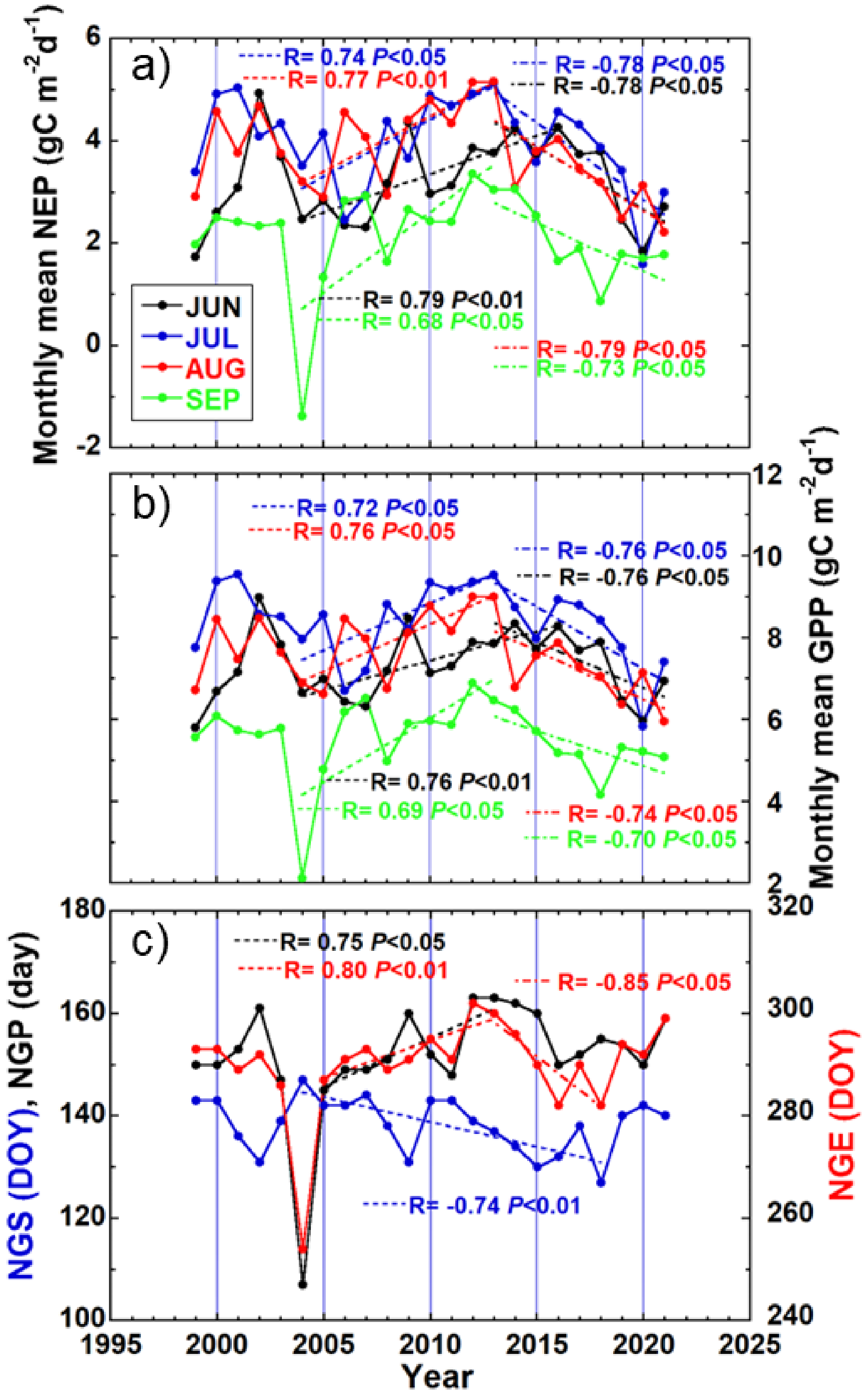

Figure 6. IAVs and significant trends of a) the monthly mean NEP, b) the monthly mean GPP of June-September, and c) the occurrences of the NGS (blue) and the NGE (red) and the length of the NGP (black).

Figure 7 shows IAVs in monthly mean LAI, SR and daytime (11:00-17:00 local time) vaper pressure deficit (VPD) from June to September, together with spring (from March to May) and August mean air temperatures. The LAI decreased from 2003 to 2004 due to the typhoons in 2004 (Fig. 7a). After this, while showing some fluctuations, the LAI gradually increased as the forest canopy recovered, and showed significantly increasing trends for each month of July to

September in 2004-2013 and for June in 2004-2016; the significant increase in the NEP and GPP trends were also observed for 2004-2013, as described above. During the period of 2013-2021, when significant decrease in the NEP and GPP trends were observed, the mean LAI for July and August maintained high values. The low LAI value in September 2018 was caused by a typhoon; however, the September value showed a significantly decreasing trend for September during 2013-2018.

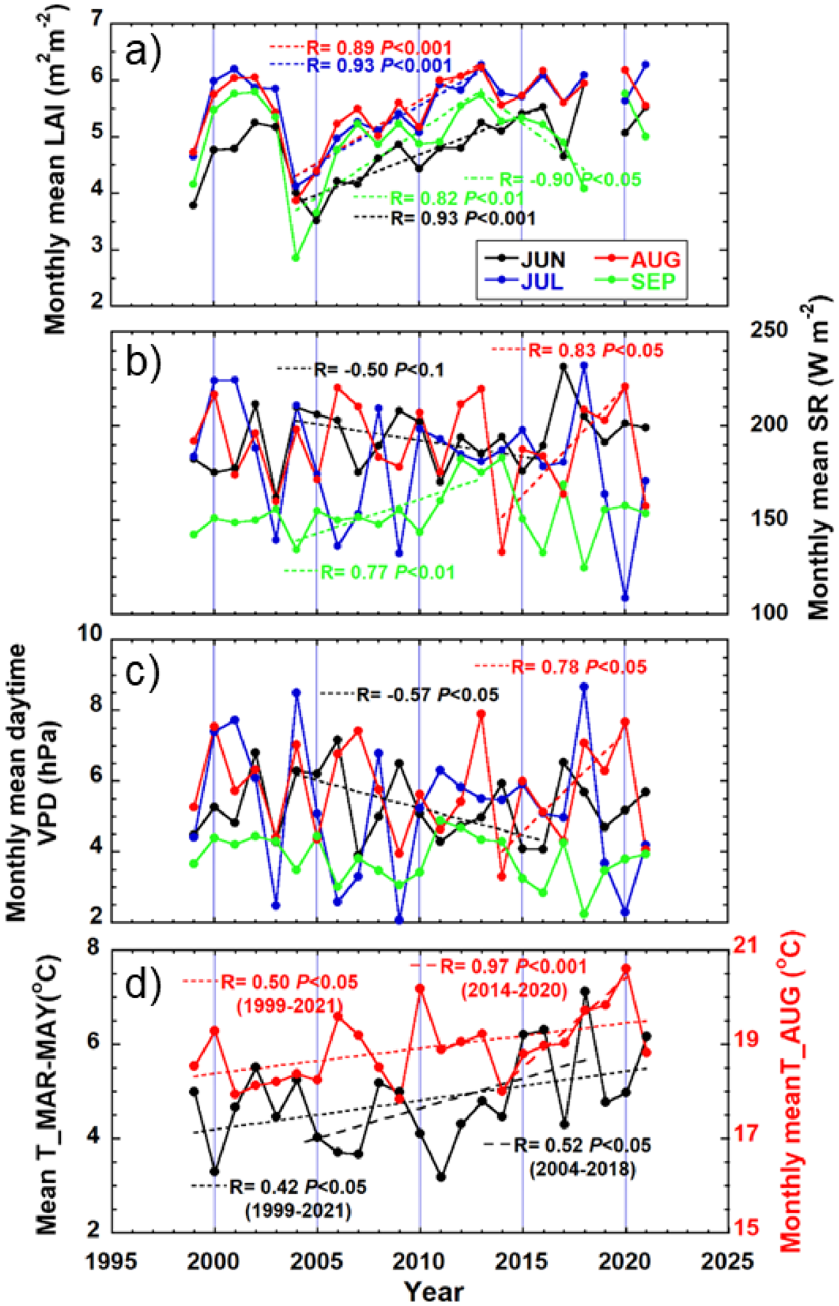

Figure 7. IAVs and significant trends in a) the monthly mean LAI, b) the monthly mean solar radiation, c) the monthly mean daytime (11:00-17:00) VPD of June-September, and d) the spring (from March to May) mean and the August monthly mean air temperatures.

The monthly mean SR in September and the mean air temperature in spring (from March to May) also showed significantly increasing trends in 2005-2013 and in 2004-2018 (also in 1999-2021), respectively (Figs. 7b and d), while the decreasing trends of the monthly mean SR and daytime VPD in June were found in 2004-2016 (Figs. 7b and c). Using the F-test, the IAVs (1σ) in the monthly mean SR were found to be significantly larger in 2014-2021 than in 2005-2013 for August ($P < 0.01$) and for July and September ($P < 0.05$) (Fig. 7b). The monthly mean air temperature in August also showed a significantly increasing trend in 1999-2021 (Fig. 7d) and a rapidly increasing trend especially in 2013-2020, accompanied by significantly increasing trends of the monthly mean SR and daytime VPD for the month (Figs. 7b and c).

5. Discussion

5. 1. IAV in annual carbon budget

Baldocchi et al. (2018) reported in their review paper that the average of the IAV (1σ) in the annual NEE was close to 100 gC m^{-2} yr^{-1} for long-term EC observations at temperate deciduous forest sites. There are various factors governing the IAV calculated from long-term observations (e.g., Froelich et al., 2015; Urbanski, et al., 2007). Among them, Baldocchi et al. (2018) identified the IAV in the length of the growing season to be a dominant factor affecting the IAV in annual NEP across much of the deciduous forests influenced by drastic changes in meteorological conditions that influence phenology of plant photosynthesis (e.g., Wilson et al. 2000; Muraoka et al. 2010).

For the TKY deciduous forest site, the IAV (1σ) in the annual NEP in 1999-2021 (83 gC m^{-2} yr^{-1}) was found to be within range of the published results. The IAV in annual NEP largely depended on the IAV in annual GPP (Fig. 2). Furthermore, the concept developed from Fig. 3 is supported by the significantly positive correlations of the IAVs in annual NEP and GPP with the IAVs in monthly mean NEP and GPP of each month from June to September (Subsection 4.1, Fig. 4) and the length of NGP (Subsection 4.2, Table 3). The significantly positive correlations with the IAVs in the monthly mean LAI of each month from June to September also suggested that the IAV in LAI during the growing season also had much influence on the IAVs in annual NEP and GPP (Subsection 4.1, Table 2). Although some significant correlations of the IAVs in NGS and NGE were found with those in annual NEP and GPP, each of the IAVs in NGS and NGE did not so strongly govern those in annual NEP and GPP as that in NGP.

With respect to the IAVs in the monthly mean NEP and GPP from June to September, it was found from significant correlations for most of these months (Tables 1 and 2) that the IAVs in the monthly mean SR and LAI from summer to early fall were likely to be important factors governing the CO_2 uptake variability by the forest ecosystem for the corresponding months. However, for the monthly mean SR of June, the correlations were not very significant with the monthly NEP and GPP. In June, LAI rapidly increases and does not yet reach the annual maximum value as shown in Fig. S1. The coefficient of variation (CV; the ratio of the standard deviation to the average) of the monthly mean SR for June is smaller than those for July, August and September (Fig. 8b). This may result in the relatively weak correlations of the IAVs in the monthly mean NEP and GPP with that in the monthly mean SR for June (Table 1).

Significance of the correlations of the IAVs in annual NEP and GPP with those in monthly mean LAI of each month from June to September (Table 2), NGP and NGE (Table 3) were largely diminished for 1999-2021 compared to 1999-2017. Also, significance of the correlations of the IAVs in corresponding monthly mean NEP and GPP with those in monthly mean SR in August (Table 1) and LAI for each month from June to August (Table 2) were even lower for 1999-2021 than for 1999-2017. These will be discussed in Subsection 5.2.

The significant correlations shown in Table 3 indicate that the IAVs in the mean air temperature in spring (March-May) and the occurrence of LE_{CET} are dominant environmental drivers for the IAV in NGS; the IAV in LE_{LAI} was not considered to be the driver since the occurrence of NGS was earlier than that of LE_{LAI} in most of the years for 1999-2021 (Fig. 5), though a significant correlation in IAV was also shown between NGS and that of LE_{LAI}. Warmer spring leads to an earlier LE of canopy trees and an earlier start of enhancement of photosynthetic activities including understory dwarf bamboo, resulting in an earlier occurrence of NGS. On the other hand, since higher SR and LAI in early fall (September) and later occurrence of LF_{LAI} maintain higher photosynthetic activities of the ecosystem in the growing season, these factors lead to a later occurrence of NGE. Since photosynthesis was fairly suppressed around the time of LF_{CET}, the correlation is considered to be weak. Thus, warmer spring and higher SR and LAI in early fall (September) expanded the length of NGP, resulting in significant correlations of the IAV in NGP with these factors.

Saigusa et al. (2005) demonstrated that the IAV in annual NEP was positively correlated with the IAV in monthly mean air temperature in April in 1994-2002 at TKY, suggesting that a warmer spring causes earlier LE, resulting in increased annual NEP. However, no significant correlation (R = 0.04) was found in this study using a longer dataset of 1999-2021, though the IAV in spring mean air temperature was indirectly correlated with that in the annual NEP via significant correlation with the IAVs in the NGS and NGP. However, a significant positive correlation of the IAV in annual NEP was found with that in monthly mean SR in September (R = 0.46, $P < 0.05$ for 1999-2021 and R = 0.59, $P < 0.01$ for 1999-2017) from our long-term data (Figs. 2, 7 and S6). The result was consistent with the fact that the IAV in monthly mean SR in September was significantly positive correlated with those in monthly mean NEP in September and NGP, each of which showed a significantly positive correlation with that of annual NEP, as described in Subsections 4.1 and 4.2. Different results between our study and Saigusa et al. (2005) highlight the possibility that the degree of importance of identified ecosystem processes contributing to the IAV in the annual carbon budget can be a function of the length and data period of analysis. Therefore, it is important to identify any “unusual” environmental event in an analysis, particularly for an analysis of a short dataset.

5.2. Trend of annual carbon budget

An increasing trend of annual NEP has been observed at some forest sites (e.g., Urbanski et al., 2007; Froelich et al., 2015). For the TKY site, no significant trend of annual NEP was detected over the observed period. However, significant increasing trends were observed for annual NEP and GPP and monthly mean NEP and GPP of each month from July to September for 2004-2013 and June monthly mean NEP and GPP for 2004-2016, while significant decreasing trends of annual NEP and GPP and monthly mean NEP and GPP of each month from June to September were detected for 2013-2021 (Figs. 2, 7a and b; subsection 4.3). From comparative analyses (Figs. 7 and 8), the following observations can be drawn: (1) The above-mentioned increasing trends nearly synchronized with the increasing trend of LAI associated with the recovery from typhoon strikes in 2004. In addition to this, the increasing trends were also probably influenced by the NGP trend related to increasing trends of mean air temperature in spring (March-May) and monthly mean SR in September; they lead to a significant trend towards earlier occurrence of NGS and a delayed trend of NGE, respectively, which are consistent with the relationship of these meteorological parameters with NGS, NGE and NGP described in Subsection 4.2. (2) Although what factors caused the latter decreasing trends was not so clearly identified, the decreasing trends may be partly attributed to a significant trend towards earlier occurrence of NGE and a significantly decreasing trend of monthly mean LAI in September in 2013-2018 and fairly low SR observed in some months from summer to early fall for 2014-2020 such as in August 2014, September 2018 and July 2020 (significant larger IAV in SR in 2014-2021 than in 2005-2013 as described above).

Since the variability patterns of the monthly mean NEP and GPP were very similar, we further investigated the decreasing trends of the monthly mean GPP for 2013-2021. For the analysis, we simply obtained the following linear functions of the observed monthly mean SR (x) and LAI (y) which simulate the monthly mean GPP (z) for each month from June to September using a multiple regression analysis for the observed data in 1999-2013 when the decreasing trends had not yet appeared:

$$z = a_i + b_i \cdot x + c_i \cdot y \qquad , (11)$$

where a, b and c are constants and the subscript i denotes each month from June to September. The reason why Eq. 11 is a function of monthly mean SR and LAI is that the IAVs in monthly mean GPP were highly correlated with the IAVs in these parameters in many of the months, as shown in Tables 1 and 2. We simulated the monthly mean GPP of each of the months from 1999 to 2021 except for 2019 (because of no available LAI data), and compared with the observed GPP. The result is given in Fig. 8. Since RMSE values of the simulation for June, July, August and September of 1999-2017 (0.39, 0.51, 0.38 and 0.55 gC m^{-2} yr^{-1}, respectively) were close to those of 1999-2013 (0.37, 0.50, 0.39 and 0.57 gC m^{-2} yr^{-1}, respectively), the relationship obtained from the 1999-2013 data are considered to be applicable up to 2017. However, the observed GPP values were noticeably smaller than the simulated values from 2018 to 2021, especially for June to August. The result suggests that the prior relationship between the IAV in GPP and its causative factors changed after 2017. This result may also be related to the facts that the significance of some of the correlations for 1999-2021 shown in Tables 1-3 was largely diminished compared to 1999-2017, as described in Subsection 5.1. High monthly mean temperatures in July 2018 and August of 2018-2020 (the highest monthly average temperatures in the top six for 1994-2021 were observed in these months), high monthly mean daytime VPD during the same months and the record low monthly SR and high monthly precipitation (>1000 mm) in July 2020 were observed. The record-breaking heatwave also dominated over Japan and Korea from mid-July to early August 2018, and it has been pointed out that it may have decreased GPP in the area during the period (Yamamoto et al., 2023). The area around TKY has humid and cool summer due to Asian Monsoon and high altitude. Therefore, a decrease in GPP due to hot and dry weather had barely been observed at TKY. However, such recently frequent occurrences of extreme weather may suppress photosynthetic activities and have altered the past relationship. To clarify the mechanism of the recent decreasing trends, further analyses and data accumulation are necessary, which probably contribute to better understanding of the impacts of climate change on the forest ecosystem at TKY.

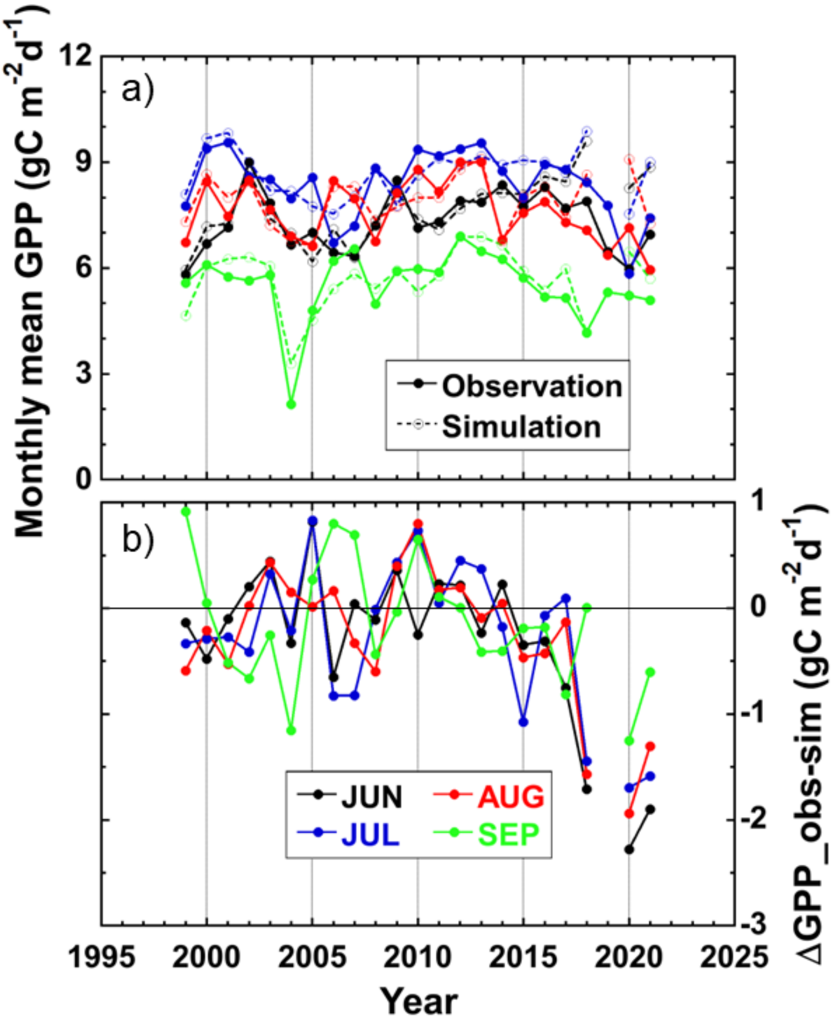

Figure 8. a) Comparison of IAVs in the monthly mean GPP of June-September between the observation and the simulation based on a multiple regression analysis, and b) IAVs in difference of the monthly mean GPP between the observation and the simulation.

5.3. Influence of interseasonal factors on IAV in carbon budget components

We further examined relationships between the variations in some of the factors, especially between those in phenomena occurring in different seasons, and their influences on the IAV in the carbon budget components at TKY. A significantly positive correlation was found between IAVs of NGS and NGE in 1999-2021 (Table 4, Fig. S7a), which indicates that NGE tends to occur early in the same year of early occurrence of NGS and vice versa. It is interesting to note that such a significant correlation of the IAVs can be seen in different seasons. As described in Subsections 4.2 and 5.1, the IAVs in NGS and NGE showed significantly positive correlations with those in LE (LE$_{LAI}$ and LE$_{CET}$) and LF$_{LAI}$, respectively, suggesting that the IAVs in NGS and NGE are influenced by variability in the forest canopy phenology. The IAVs in LE$_{LAI}$ and LE$_{CET}$ were also positively correlated with those in LF$_{LAI}$ and LF$_{CET}$, respectively (Table 4, Figs.

S7b and c), showing that LF tends to occur early in the same year of early occurrence of LE and vice versa. Therefore, the positive correlation between NGS and NGE observed at TKY may be attributed to such interseasonal-phenological characteristics at the site. Some recent studies also found that earlier/later LF is associated with earlier/later LE at some temperate deciduous forests, and pointed out that winter-spring warming due to climate change will not always lead to extension of the growing season into the future (Fu et al., 2014; Keenan & Richardson, 2015; Piao et al., 2019b; Zani et al., 2020).

Table 4. Correlation coefficients (R) of IAVs between interseasonal parameters for each period.

Interseasonal parameter	Period	R
NGS vs. NGE	1999-2021	0.37*
$\mathrm{LE}_{\mathrm{LAI}}$ vs. $\mathrm{LF}_{\mathrm{LAI}}$	1999-2021	0.50**
$\mathrm{LE}_{\mathrm{CET}}$ vs. $\mathrm{LF}_{\mathrm{CET}}$	1999-2021	0.39*
T_Spring vs. SR_September	1994-2021	-0.33*

Note: T_Spring and SR_September represent mean T from March to May and monthly mean SR in September, respectively. The data for 2004 are excluded for the analysis of NGS vs. NGE, $\mathrm{LE}_{\mathrm{LAI}}$ vs. $\mathrm{LF}_{\mathrm{LAI}}$ and $\mathrm{LE}_{\mathrm{CET}}$ vs. $\mathrm{LF}_{\mathrm{CET}}$. The data for 2019 are also excluded for the analysis of $\mathrm{LE}_{\mathrm{LAI}}$ vs. $\mathrm{LF}_{\mathrm{LAI}}$. * and ** represent statistical significance of correlations for $0.1 < P \leq 0.05$ and $0.05 < P \leq 0.01$, respectively.

On the other hand, significant correlations in the IAV were also found between meteorological parameters observed in different seasons at TKY. A negative correlation of the IAV in the mean air temperature in spring (March-May) was seen with the IAV in the monthly mean SR in September (Table 4, Fig. S7d). The relationships of the IAVs in these meteorological parameters with those in NGS, NGE and NGP were described in Subsection 4.2. From these relationships, it is suggested that early/late occurrence of NGS and long/short NGP related to high/low temperature in spring tend to be accompanied with early/late occurrence of NGE and short/long NGP related to low/high SR in early fall in the same year. Therefore, the positive correlation between NGS and NGE observed at TKY may also be influenced by such an interseasonal relationship of the meteorological parameters at the site. Whichever process caused the positive correlation between NGS and NGE, these opposite effects on the length of NGP of the year partly offset each other and the difference between the two effects may cause the IAV in NGP. Such a mechanism of the IAV in NGP probably affects those in annual NEP and GPP at TKY.

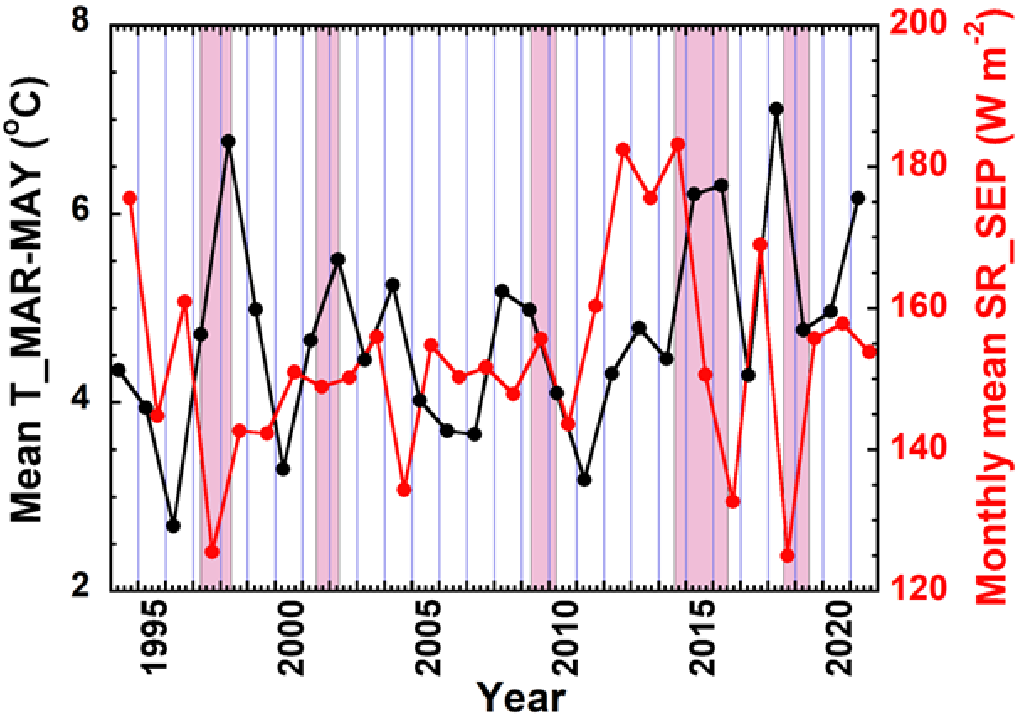

Figure 9. IAVs in mean air temperature from March to May (black) and solar radiation in September (red). Pink-shades represent El Niño periods.

High temperature anomaly from winter to spring and low temperature and low SR anomaly from summer to fall tend to be observed during the El Niño period in Japan (Saigusa et al., 2005; https://ds.data.jma.go.jp/tcc/tcc/products/climate/ENSO/elnino.html). Figure 9 shows the IAVs in the mean air temperature in spring and the monthly mean SR in September observed at TKY, along with the recent El Niño periods (https://www.data.jma.go.jp/tcc/tcc/products/elnino/ensoevents.html). The IAVs in these parameters seem to reflect such meteorological characteristics in Japan during the El Niño period, except for a few cases. Therefore, the above-mentioned interseasonal relationship of the meteorological parameters observed at TKY is considered to be likely influenced by the ENSO events. Using an earlier observational data, Saigusa et al. (2005) pointed out the influence of El Niño on the canopy phenology and the carbon budget of the forest ecosystem at TKY. The present study also suggests that the IAVs in the phenology and the carbon budget obtained from our long-term observation were influenced by ENSO events. Many studies reported that hot and dry weather conditions associated with El Niño events often cause drought and forest fires in wide areas such as Southeast Asia and South America, leading to enhancement of CO_2 release from global terrestrial biosphere (e.g., IPCC, 2021; Rödenbeck et al., 2018; Liu et al., 2017; Goto et al., 2017). However, this is not the case for TKY, since different weather conditions such as wet and cloudy summer-early fall and warm winter-spring tend to be observed around our site during the El Niño period.

6. Summary

We initiated a long-term measurement of CO_2 flux between the atmosphere and the forest ecosystem in September of 1993 at TKY in a cool-temperate deciduous forest in central Japan. In this paper, we reanalyzed the long-term data mainly obtained from the EC measurements obtained during 1999-2021. The IAVs and the trends of annual carbon budget components were examined, and then their environmental factors were investigated.

The main results obtained from the analyses are as follows:

(1) The annual NEP, GPP and Rec (mean ± 1σ) for the EC measurement period were 265 ± 86, 1066 ± 91, and 801 ± 21 gC m^{-2} yr^{-1}, respectively. The IAV in the annual NEP strongly depended on the IAV of annual GPP.

(2) Based on the significant correlations with the IAVs in monthly mean NEP, GPP and LAI for each month from June to September, the IAVs in annual NEP and GPP largely depended on those in NEP, GPP and LAI from summer to early fall. The IAVs in the monthly mean NEP and GPP were attributed to those in the monthly mean SR from July to September and those in the monthly mean LAI from June to September for the respective months.

(3) The IAVs in the annual NEP and GPP were governed by the IAV in NGP. Early/late occurrence of NGS was attributed to warm/cold spring and early/late occurrence of LE_{CET}, while late/early occurrence of NGE was associated with high/low monthly mean SR in September and late/early LE_{LAI}. Early NGS and/or late NGE led to long NGP.

(4) Significant increasing and decreasing trends of annual NEP and GPP were detected in 2004-2013 and 2013-2021, respectively. The former increasing trends were highly linked to recovery from the ecosystem disturbances due to typhoon strikes in 2004, and partly related to trends of some meteorological parameters. On the other hand, the cause of the latter decreasing trends was not clearly identified though the decreasing trend of the monthly mean LAI in September and the trend towards earlier occurrence of NGE for 2013-2018 may partly be related to them.

(5) The above-mentioned decreasing trends of annual NEP and GPP and the noticeably diminished significance seen in the correlations of the IAVs in carbon budget components with those in some environmental factors for 1999-2021 compared to 1999-2017 may have been influenced by the recent extreme weather conditions, such as high temperatures in August for 2018-2020 and the record high monthly precipitation and low monthly SR in July 2020.

(6) Some intercorrelations of IAV between the events occurring in different seasons, such as the occurrences of NGS and NGE and the occurrences of LE and LF, were found. It was suggested that they may be attributed not only to some biological functions but also to meteorological parameters associated with ENSO events, which could have influence on annual carbon budget at TKY.

Some of the results obtained from the long-term measurement were found to be different from those shown in the previous studies that were based on shorter observation. Also, decadal scale phenomena such as increasing and decreasing trends of annual NEP and GPP could not be detected without the long-term observation. Therefore, long-term observations are very important for better understanding of the carbon cycle in forest ecosystems. Collaboration with studies using various approaches such as biometric measurements (Ohtsuka et al., 2009) and model simulations (Ito et al., 2010b; Higuchi et al., 2005) should be further developed. Such multidisciplinary studies based on long-term observations are essential to precisely predict responses of the terrestrial biosphere to climate change.

Acknowledgements

We would like to thank N. Nishimura, H. Koizumi, T. Akiyama, I. Tamagawa, K. Kurumado, S. Yoshitake, K. Suzuki, H. Hiratsuka, and members of the River Basin Research Center of Gifu University for their cooperation. We are also very grateful to K. Muto, H. Yatabe and Y. Takeda of National Institute of Advanced Industrial Science and Technology and A. Kudo and C. Abe of Japan ANS Co. Ltd. for their support to observation and data analyses. This study was partly supported by the JSPS KAKENHI (Grant Numbers JP24241008, JP24310017, JP15H02814, JP26241005, JP18H03365, JP19H03301, JP19H01975, JP21H05316, JP21H05312, JP22H00564 and JP22H05006) and the Global Environment Research Coordination System from the Ministry of the Environment, Japan (Grant Numbers MAFF0751, MAFF1251, MAFF2254), the Global Environment Research Fund of the Ministry of the Environment, Japan (S-1: Integrated Study for Terrestrial Carbon Management of Asia in the 21st Century Based on Scientific Advancement).

Data Availability Statement

The dataset of the carbon budget at TKY presented in the manuscript has been made publically available at https://doi.org/10.5281/zenodo.8300684.

References

Baldocchi, D., Falge, E., Gu, L., Olson, R., Hollinger, D., Running, S., et al. (2001). FLUXNET: A new tool to study the temporal and spatial variability of ecosystem-scale carbon dioxide, water vapor, and energy flux densities. *Bull. Amer. Meteorol. Soc.,* 82, 2415-2434, https://doi.org/10.1175/1520-0477(2001)082<2415:FANTTS>2.3.CO;2.

Baldocchi, D., Housen, C., & Reichstein, M. (2018). Inter-annual variability of net and gross ecosystem carbon fluxes: A review. *Agric. For. Meteorol.,* 249, 520-533, https://doi.org/10.1016/j.agrformet.2017.05.015.

Friedlingstein, P., O'Sullivan, M., Jones, M. W., Andrew, R. M., Gregor, L., Hauck, J., et al., (2022). Global Carbon Budget 2022. *Earth Syst. Sci. Data,* 14, 4811–4900, https://doi.org/10.5194/essd-14-4811-2022.

Froelicha, N., Croft, H., Chen, J. M., Gonsamo, A., & Staebler, R. M. (2015). Trends of carbon fluxes and climate over a mixed temperate–boreal transition forest in southern Ontario, Canada. *Agric. For. Meteorol.,* 211-212, 72-84, https://doi.org/10.1016/j.agrformet.2015.05.009.

Fu, Y. S. H., Campioli, M., Vitasse, Y., Boeck, H. J. D., Berge, J. V. d., AbdElgawad, H., et al. (2014). Variation in leaf flushing date influences autumnal senescence and next year's flushing date in two temperate tree species. *Proc. Natl. Acad. Sci.,* 111, 7355–7360, https://doi.org/10.1073/pnas.1321727111.

Goto, D., Morimoto, S., Ishidoya, S., Aoki, S., & Nakazawa, T. (2017). Terrestrial biospheric and oceanic CO_2 uptakes estimated from long-term measurements of atmospheric CO_2 mole fraction, $\delta^{13}C$, and $\delta(O_2/N_2)$ at Ny-Ålesund, Svalbard. *J. Geophys. Res. Biogeosci.,* 122, 1192-1202, https://doi.org/10.1002/2017JG003845.

Higuchi, K., Shashkov, A., Chan, D., Saigusa, N., Murayama, S., Yamamoto, S., et al. (2005). Simulations of seasonal and inter-annual variability of gross primary productivity at Takayama with BEPS ecosystem model. *Agri. For. Meteorol.,* 134, 143–150, https://doi.org/10.1016/j.agrformet.2005.08.018.

IPCC (2021). Climate Change 2021: *The Physical Science Basis. Contribution of Working Group I to the Sixth Assessment Report of the Intergovernmental Panel on Climate Change.* V. Masson-Delmotte, P. Zhai, A. Pirani, S.L. Connors, C. Péan, S. Berger, N. Caud, Y. Chen, L. Goldfarb, M.I. Gomis, M. Huang, K. Leitzell, E. Lonnoy, J.B.R. Matthews, T.K. Maycock, T. Waterfield, O. Yelekçi, R. Yu, & B. Zhou (eds.), 2391 pp., Cambridge University Press, Cambridge, UK and New York, USA, https://doi.org/10.1017/9781009157896.

Ishidoya, S., Murayama, S., Kondo, H., Saigusa, N., Kishimoto-Mo, A. W., & Yamamoto, S. (2015). Observation of O_2:CO_2 exchange ratio for net turbulent fluxes and its application to forest carbon cycles. *Ecol, Res.,* 30, 225–234, https://doi.org/10.1007/s11284-014-1241-3.

Ito, A. (2010a). Evaluation of the impacts of defoliation by tropical cyclones on a Japanese forest's carbon budget using flux data and a process-based model. *J. Geophys. Res.,* 115, G04013, https://doi.org/10.1029/2010JG001314.

Ito, A. (2010b). Changing ecophysiological processes and carbon budget in East Asian ecosystems under near-future changes in climate: implications for long-term monitoring from a process-based model. *J. Plant Res.,* 123, 577–588, https://doi.org/10.1007/s10265-009-0305-x.

Ito, A., Saitoh, T. M., & Sasai, T. (2015). Synergies between observational and modeling studies at the Takayama site: toward a better understanding of processes in terrestrial ecosystems. *Ecol. Res.,* 30, 201–210, https://doi.org/10.1007/s11284-014-1205-7.

Keenan, T. F., & Richardson, A. D. (2015). The timing of autumn senescence is affected by the time of spring phenology: Implications for predictive models. *Global Change Biol.,* 21, 2634–2641, https://doi.org/10.1111/gcb.12890.

Kondo, H., Saigusa, N., Murayama, S., Yamamoto, S., & Kannari, A. (2001). A numerical simulation of the daily variation of CO_2 in the central part of Japan summer case. *J. Meteorol. Soc. Jpn.,* 79, 11–21, https://doi.org/10.2151/jmsj.79.11.

Liu, J., Bowman, K. W., Schimel, D. S., Parazoo, N. C., Jiang, Z., Lee, M., et. al. (2017). Contrasting carbon cycle responses of the tropical continents to the 2015–2016 El Niño. *Science,* 358, eaam5690, https://doi.org/10.1126/science.aam5690.

Muraoka, H., & Koizumi, H. (2005). Photosynthetic and structural characteristics of canopy and shrub trees in a cool-temperate deciduous broadleaved forest: Implication to the ecosystem carbon gain. *Agric. For. Meteorol.,* 134, 39–59. https://doi.org/10.1016/j.agrformet.2005.08.013.

Muraoka, H., Saigusa, N., Nasahara, K. N., Noda, H., Yoshino, J., Saitoh, T. M., et al. (2010). Effects of seasonal and interannual variations in leaf photosynthesis and canopy leaf area index on gross primary production of a cool-temperate deciduous broadleaf forest in Takayama, Japan. *J. Plant Res.,* 123, 563–576, https://doi.org/10.1007/s10265-009-0270-4.

Muraoka, H., Saitoh, T. M., & Nagai, S. (2015). Long-term and interdisciplinary research on forest ecosystem functions: challenges at Takayama site since 1993. *Ecol. Res.,* 30, 197–200, https://doi.org/10.1007/s11284-015-1251-9.

Murayama, S., Saigusa, N., Chan, D., Yamamoto, S., Kondo, H., & Eguchi, Y. (2003). Temporal variations of atmospheric CO_2 concentration in a temperate deciduous forest in central Japan. *Tellus, Ser. B,* 55, 232–243, https://doi.org/10.1034/j.1600-0889.2003.00061.x.

Murayama, S., Takamura, C., Yamamoto, S., Saigusa, N., Morimoto, S., Kondo, H., et al. (2010). Seasonal variations of atmospheric CO_2, $\delta^{13}C$, and $\delta^{18}O$ at a cool temperate deciduous forest in Japan: Influence of Asian monsoon. *J. Geophys. Res.,* 115, D17304, https://doi.org/10.1029/2009JD013626.

Musavi, T., Migliavacca, M., Reichstein, M., Kattge, J., Wirth, C., Black, T. A., et al. (2017). Stand age and species richness dampen interannual variation of ecosystem-level photosynthetic capacity. *Nature Ecol. Evol.*, 1, 0048, https://doi.org/10.1038/s41559-016-0048.

Nagai, S., Saitoh, T. M., & Nasahara, K. N. (2021). How did the characteristics of the growing season change during the past 100 years at a steep river basin in Japan? *PLoS ONE,* 16, e0255078, https://doi.org/10.1371/journal.pone.0255078.

Nagai, S., Saitoh, T. M., Kurumado, K., Tamagawa, I., Kobayashi, H., Inoue, T., et al. (2013). Detection of bio-meteorological year-to-year variation by using digital canopy surface images of a deciduous broad-leaved forest. *SOLA,* 9, 106−110, https://doi.org/10.2151/sola.2013-024.

Nakazawa, T., Ishizawa, M., Higuchi, K., & Trivett, N. B. A. (1997). Two curve fitting method applied to CO_2 flask data. *Environmetrics,* 8, 889–906, https://doi.org/10.1002/(SICI)1099-095X(199705)8:3<197::AID-ENV248>3.0.CO;2-C.

Nasahara, K. N., Muraoka, H., Nagai, S., & Mikami, H. (2008). Vertical integration of leaf area index in a Japanese deciduous broad-leaved forest. *Agric. For. Meteorol.,* 148, 1136-1146, https://doi.org/10.1016/j.agrformet.2008.02.011.

Ohtsuka, T., Mo, W., Satomura, T., Inatomi, M., & Koizumi, H. (2007). Biometric based carbon flux measurements and net ecosystem production (NEP) in a temperate deciduous broad-leaved forest beneath a flux tower. *Ecosystems,* 10, 324–334, https://doi.org/10.1007/s10021-007-9017-z.

Ohtsuka, T., Saigusa, N., & Koizumi, H. (2009). On linking multiyear biometric measurements of tree growth with eddy covariance-based net ecosystem production. *Global Change Biol.,* 15, 1015–1024, https://doi.org/10.1111/j.1365-2486.2008.01800.x.

Piao, S., Qiang, L., Chen, A., Janssens, I. A., Fu, Y., Dai, J., et al. (2019b). Plant phenology and global climate change: Current progresses and challenges. *Global Change Biol.,* 25, 1922–1940, https://doi.org/10.1111/gcb.14619.

Piao, S., Wang, X., Wang, K., Li, X., Bastos, A., Canadell, J. G., et al. (2019a). Interannual variation of terrestrial carbon cycle: Issues and perspectives. *Global Change Biol.,* 26, 300–318, https://doi.org/10.1111/gcb.14884.

Reichstein, M., Bahn, M., Ciais, P., Frank, D., Mahecha, M. D., Seneviratne, S. I., et al. (2013). Climate extremes and the carbon cycle. *Nature,* 500, 287-295, https://doi.org/10.1038/nature12350.

Reichstein, M., Falge, E., Baldocci, D., Papale, D., Aubinet, M., Berbigier, P., et al. (2005). On the separation of net ecosystem exchange into assimilation and ecosystem respiration: review and improved algorithm. *Global Change Biol.,* 11, 1424–1439, https://doi.org/10.1111/j.1365-2486.2005.001002.x.

Rödenbeck C., Zaehle, S., Keeling, R., & Heimann, M. (2018). History of El Niño impacts on the global carbon cycle 1957-2017: a quantification from atmospheric CO_2 data. *Phil. Trans. R. Soc., B,* 373, 20170303, https://doi.org/10.1098/rstb.2017.0303.

Saigusa, N., Yamamoto, S., Hirata, R., Ohtani, Y., Ide, R., Asanuma, J., et al. (2008). Temporal and spatial variations in the seasonal patterns of CO_2 flux in boreal, temperate, and tropical forests in East Asia. *Agric. For. Meteorol.,* 148, 700–713. https://doi.org/10.1016/j.agrformet.2007.12.006.

Saigusa, N., Yamamoto, S., Murayama, S., & Kondo, H. (2005). Interannual variability of carbon budget components in an AsiaFlux forest site estimated by long-term flux measurements. *Agric. For. Meteorol.,* 134, 4–16. https://doi.org/10.1016/j.agrformet.2005.08.016.

Saigusa, N., Yamamoto, S., Murayama, S., Kondo, H., & Nishimura, N. (2002). Gross primary production and net ecosystem production of a cool-temperate deciduous forest estimated by the eddy covariance method. *Agric. For. Meteorol.,* 112, 203–215. https://doi.org/10.1016/S0168-1923(02)00082-5.

Saitoh, T. M., Nagai, S., Noda, H. M., Muraoka, H., & Nasahara, K. N. (2012). Examination of the extinction coefficient in the Beer–Lambert law for an accurate estimation of the forest canopy leaf area index. *For. Sci. Tech.,* 8, 67-76, https://doi.org/10.1080/21580103.2012.673744.

Urbanski, S., Barford, C., Wofsy, S., Kucharik, C., Pyle, E., Budney, J., et al. (2007). Factors controlling CO_2 exchange on timescales from hourly to decadal at Harvard Forest. *J. Geophys. Res.,* 112, G02020, https://doi.org/10.1029/2006JG000293.

Wehr, R., Munger, J. W., McManus, J. B., Nelson, D. D., Zahniser, M. S., Davidson, E. A., et al. (2016). Seasonality of temperate forest photosynthesis and daytime respiration, *Nature,* 534, 680-683, https://doi.org/10.1038/nature17966.

Wilson, K. B., Baldocchi, D. D., & Hanson, P. J. (2000), Spatial and seasonal variability of photosynthetic parameters and their relationship to leaf nitrogen in a deciduous forest. *Tree Physiol.*, 20, 565–578, https://doi.org/10.1093/treephys/20.9.565.

Wofsy, S. C., Goulden, M. L., Munger, J. W., Fan, S.-M., Bakwin, P. S., Daube, B. C., et al. (1993). Net Exchange of CO_2 in a Mid-Latitude Forest, Science, 260, 1314 – 1317, https://doi.org/10.1126/science.260.5112.1314.

Yamamoto, S., Murayama, S., Saigusa, N., & Kondo, H. (1999), Seasonal and inter-annual variation of CO_2 flux between a temperate forest and the atmosphere in Japan. *Tellus, Ser. B,* 51, 402–413. https://doi.org/10.1034/j.1600-0889.1999.00020.x.

Yamamoto, Y., Ichii, K., Ryu, Y., Kang, M., Murayama, S., Kim, S.-J., & Cleverly, J. R. (2023). Detection of vegetation drying signals using diurnal variation of land surface temperature: Application to the 2018 East Asia heatwave. *Remote Sensing of Environment*, 291, 113572, https://doi.org/10.1016/j.rse.2023.113572.

Zani, D., Crowther, T. W., Mo, L., Renner, S. S., & Zohner, C. M. (2020). Increased growing-season productivity drives earlier autumn leaf senescence in temperate trees. *Science,* 370, 1066–1071, https://doi.org/10.1126/science.abd8911.

Figure captions

Figure 1. a) Temporal variation in daily NEP (dot) and the best fit curve to the data (red line) for 1994-2021. b) Temporal variations in monthly mean daily NEP (red line), Rec (black line) and GPP (blue line) for the same period.

Figure 2. Temporal variations in annual NEP, Rec and GPP. The data were obtained by using an aerodynamic (AD) method and an eddy-covariance (EC) method until July 1998 and after that, respectively.

Figure 3. Schematic diagram showing factors governing the IAV in annual NEP; a) the IAV in the magnitude of the NEP during the summertime, and b) that in the length of the period (NGP) showing positive NEP values (between the NGS and the NGE).

Figure 4. Correlation coefficients (R) of the IAV between annual NEP and monthly mean NEP for each month for 1999-2021 (green and black vertical bars), and the averages of monthly mean NEP for each month over 1999-2021 (red closed circles) along with the standard deviation (1σ) from the average values (red vertical lines). The green bars represent significant correlations at >99% confident levels.

Figure 5. IAVs in occurrences of NGS, NGE, LE_{LAI}, LF_{LAI}, LE_{CET} and LF_{CET}. LE_{LAI} and LF_{LAI} for 2019 are not plotted because of no available LAI data.

Figure 6. IAVs and significant trends of a) the monthly mean NEP, b) the monthly mean GPP of June-September, and c) the occurrences of the NGS (blue) and the NGE (red) and the length of the NGP (black).

Figure 7. IAVs and significant trends in a) the monthly mean LAI, b) the monthly mean solar radiation, c) the monthly mean daytime (11:00-17:00) VPD of June-September, and d) the spring (from March to May) mean and the August monthly mean air temperatures.

Figure 8. a) Comparison of IAVs in the monthly mean GPP of June-September between the observation and the simulation based on a multiple regression analysis, and b) IAVs in difference of the monthly mean GPP between the observation and the simulation.

Figure 9. IAVs in mean air temperature from March to May (black) and solar radiation in September (red). Pink-shades represent El Niño periods.

Table captions

Table 1. Correlation coefficient of IAVs of monthly mean SR in June, July, August and September with those of monthly mean NEP and GPP for the respective months in1999-2021 and 1999-2017 except for 2004.

Table 2. Correlation coefficients (R) of IAV in monthly mean LAI for each of June, July, August and September with those in monthly mean NEP and GPP for the respective months and with those in annual NEP and GPP in the same year in 1999-2021 except for 2019 and in 1999-2017.

Table 3. Correlation coefficient (R) of IAVs in NGS, NGE and NGP with those of annual NEP

and GPP and environmental factors for 1999-2021 and 1999-2017.

Table 4. Correlation coefficients (R) of IAVs between interseasonal parameters for each period.